ORIGINAL ARTICLE

How modernized and strengthened GPS signals enhance the system performance during solar radio bursts

Yu. V. Yasyukevich[1] · A. S. Yasyukevich[1] · E. I. Astafyeva[2]

Abstract

A Solar Radio Burst (SRB) is one of the most severe natural hazards affecting the performance of the global navigation satellite systems (GNSS). Considering the influence of different threat factors, the GNSS developers upgrade the systems to amend the accuracy and noise-proof features of the systems. In particular, GPS gradually replaces "old" satellites (GPS IIA, GPS IIR-A, GPS IIR-B) with new-generation equipment (GPS IIR-M, GPS IIF, GPS III) featured by an increase in the emitted signal power at L2 frequency and by new civilian codes. In this work, based on examples of the extreme SRB of September 24, 2011, and the severe SRB of September 6, 2017, we study how such modernization can improve the GPS system performance during solar flares accompanied by intense SRB. We recorded SRB-related drops in signal strength (S), which were 7.5/0 dB-Hz for the S1C, 10/7 dB-Hz for the S2X, 17/8 dB-Hz for the S2W and 9/7.5 for the S5/S5X in 2011/2017 correspondingly. The drop in the S2W signal strength for the modernized blocks was comparable in amplitude to those of the "old" blocks. However, the modernized IIR-M/IIF blocks were featured by about 5 dB-Hz higher signal strength. This resulted in a double and triple decrease in loss-of-lock density for the IIR-M/IIF satellites in 2011 and 2017, respectively, as compared to IIA/IIR-A during SRBs. Therefore, the increase in the emitted signal power and new civilian codes potentially enhance the stability of the GPS operation.

Keywords Global navigation satellite systems (GNSS) · GPS · Solar radio burst · Signal power · Signal loss-of-lock

Introduction

Global navigation satellite systems (GNSS) have been widely implemented in different fields of industry and transportation. Nowadays, several GNSS are in operation—the American GPS, Russian GLONASS, European Galileo, and the Chinese BeiDou. Therefore, requirements for the accuracy and reliability of GNSS have continuously grown. The performance quality of these systems largely depends on the propagation medium, i.e., on the ionosphere. Irregularities of the ionospheric plasma density may significantly affect radiowave propagation, causing rapid phase and amplitude fluctuations (radio scintillations), or even cause loss of lock (LoL) of satellite signals. These may lead to a significant degradation in system performance, accuracy, and reliability.

Geomagnetic storms are one of the causes of the occurrence of the ionospheric irregularities that lead to the worsening of GNSS performance quality. Afraimovich et al. (2003) showed that, during geomagnetic storms, the standard deviation in the position determination increased for all types of GPS receivers. Astafyeva et al. (2014) demonstrated that the number of GPS Losses-of-Lock increased drastically during storms and especially during super-storms. Thus, we are in obvious need of the development of specific space-weather monitoring services that could lead to improving current positioning applications based on GNSS (Jakowski et al. 2005).

A more detailed overview of space weather effects on GNSS performance and ionospheric total electron content (TEC) can be found in Coster and Komjathy (2008) and

✉ A. S. Yasyukevich
annpol@iszf.irk.ru

E. I. Astafyeva
astafyeva@ipgp.fr

1   Institute of Solar-Terrestrial Physics SB RAS, Lermontov str., p/o box 291,126a, Irkutsk, Russia 664033

2   Université de Paris, Institut de Physique du Globe de Paris (IPGP), 35-39 Rue Hélène Brion, 75013 Paris, France

Afraimovich et al. (2013). A brief review of solar flare effects on the ionosphere is provided in Tsurutani et al. (2009).

Solar radio bursts (SRB) that occasionally accompany solar flares are among the most severe disturbing natural factors for satellite radio technical systems. Klobuchar et al. (1999) predicted that SRBs could affect the GPS performance if the solar flux in the L band frequency range exceeded a threat threshold of about 40,000 solar flux units (sfu). Further studies by Chen et al. (2005) and Demyanov et al. (2013) proved that even weaker solar radio bursts are capable of causing GNSS malfunction. For instance, Chen et al. (2005) showed that almost no GPS L2 signals were tracked around the subsolar area during the October 28, 2003 SRB, although the burst flux density at 1415 MHz was only 4000–12,000 sfu, which is far below the "threat" threshold previously suggested by Klobuchar et al. (1999).

Cerruti et al. (2006) investigated the carrier-to-noise ratio during the September 2005 SRB. They showed that the maximum degradation at GPS L1 reached about 3.0 dB, while at the semi-codeless L2 signal degradation of 10.0 dB was observed.

Carrano et al. (2009) showed that under the direct effect of 10,000–1,000,000 sfu solar radio emission, the signal-to-noise ratio (SNR) can decrease by 10–30 dB at the navigation receiver antenna. Consequently, loss of signal tracking was detected for many navigation satellites at the earth sunlit part for a rather long time (up to 1 hour). Carrano et al. (2009) showed that SNR reduction experienced by a GPS receiver depends on the solar incidence angle due to the antenna gain anisotropy.

Muhammad et al. (2015) showed that during the September 24, 2011, extreme SRB event, the GPS carrier-to-noise density ratio (C/N0) reduced at most by 13 dB at L1 and 24 dB at L2. The C/N0 degradation induced the loss of lock at GPS L1 and L2 frequencies and significant code-tracking errors. For the same 2011 SRB event, Sreeja et al. (2013) showed the maximum carrier-to-noise density ratio reductions of 11.0, 22.0, and 10.0 dB-Hz for the GPS L1C/A, L2P, and L2C signals, respectively. Degradation in the positioning accuracy in the PPP regime during SRB flares was revealed in Sreeja et al. (2014) and Yasyukevich et al. (2018a).

Sato et al. (2019) pointed out that the degradation of GNSS performance during a flare depends on frequency. For the September 6, 2017 SRB, the authors recorded the impact of the burst at L2 and L5 frequencies, but not at L1 frequency. The maximum signal-to-noise ratio reduction of −10 dB was observed when the solar radio flux pulsated around a level of 2000 sfu. An analysis of the flare impact on the ionosphere and GNSS precise positioning (PPP) and navigation support services have been performed by Berdermann et al. (2018). They revealed that not only the GNSS

PPP service was affected during the flare, but so was the EGNOS system.

A sudden increase in the total electron content (SITEC) caused by intense EUV flux during solar flares is another potential factor worsening the GNSS in terms of positioning accuracy (Matsoukas et al. 1972). SITEC may dramatically affect the positioning precision by GNSS methods, as was shown in Zhang and Xiao (2005) and Wan et al. (2005). Sudden rapid growth in TEC (and even more importantly, its second phase derivative) could also potentially result in losses of lock. However, only very intensive EUV events, such as the October 28, 2003 flare, when the SITEC exceeded 3 TECU/min (Zhang and Xiao 2005), can induce the TEC to increase high enough to cause LoLs. In comparison, the September 6, 2017, flare only caused a TEC increase of about 1.5 TECU/min in the subsolar sector (Yasyukevich et al., 2018a, b). Moreover, the ionospheric density enhancement during the 2017 solar flare depended on the solar zenith angle: larger enhancement (and larger SITEC) corresponded to smaller solar zenith angle (Zhang et al. 2019). Previous work also reported that SITEC played a secondary role in losses of signal lock (Chen et al. 2005). Rodríguez-Bilbao et al. (2015) concluded that the SITEC was a primary source for large errors observed in PPP during the October 28, 2003 flare, while the cycle slips or complete signal loss had been attributed to an SRB that took place on the same day. Sato et al. (2019) and Berdermann et al. (2018) also concluded that the positioning error referred instead to the extreme solar ultraviolet than to solar radio interferences. The authors also noted that a combination of EUV and SRB impact on GNSS signals is possible.

The power of the radio signal emitted by satellites is one of the decisive factors that impact the quality of the estimated radio navigation parameters. As shown repeatedly (Zakharov et al. 2016; Jin and Oksavik 2018), navigation signal cycle slips occur mainly at the L2 GPS frequency due to two factors: lower transmitter power at L2 and unknown code structure of GPS P(Y) code. To improve this issue, GNSS developers currently upgrade the systems to amend the accuracy and noise-proof features of the systems by improving the ephemeris time support, by increasing the number of navigation signals available to the civilian consumer, and by improving the structure of these signals. Thus, in the GPS system, the satellites have been one-by-one replaced with new-generation modernized GPS satellites (GPS IIR-M, GPS IIF, GPS III) that possess improved characteristics in terms of noise immunity. Another factor in improving system stability is a receiver hardware advancement. Fortes et al. (2015) showed that hardware receiver technology advancements decreased the percentage of L2 loss of lock by a factor of 3 considering the hardware/firmware models used in 2002 and 2012.

This work analyzes how the change in the emitted GPS satellite signal power affects the system performance stability during solar flares accompanied by intense SRB. In addition, we analyze how new civilian codes can increase the stability of GPS operation during SRB.

GPS signals and their modernization

Currently, GPS satellites can emit 5 civilian ranging codes: C/A at L1, L2C (M and L codes) at L2, as well as I5 and Q5 codes at L5. The most modern receivers can also semi-codelessly track protected P(Y) signals at L1 and L2. Z-tracking (Ashjaee and Lorenz 1992) is usually assumed to be the best tracking procedure for the P(Y) signal. The z-tracking results in equal (or almost equal) signal strength at L1 and L2. However, there is a 13 dB decrease in signal-to-noise under semi-codeless z-tracking compared to code tracking (Hofmann-Wellenhof et al. 2008).

According to the GPS interface control document (IS-GPS-200J, 2018), the power of the GPS signal emitted by the modernized satellite blocks, starting with the IIR-M, was increased to respond to the requirements for the minimum received signal power at a ground-based receiver. Table 1 lists the minimum power values received at ground-based receivers for various types of GPS satellites. One can see that starting with the IIR-M block, the minimum signal power guaranteed by the system at the L2-frequency increased by 3–5 dBW. In addition, for GPS satellites equipped with IIR-M and IIF blocks, there is a possibility to redistribute the transmitting power between the signals.

In the current research, we study S1C, S2W, S2X and S5X observables, while the main attention is devoted to the S1C and S2W because P1C and P2W currently are the main observables for civilian navigation. S1C stands for the code C/A tracking at L1, S2W for the semi-codeless L2 P(Y) z-tracking, S2X for code M+L L2 tracking, and S5X for the code I+Q L5 tracking.

Table 1 Minimum signal power received at a ground-based receiver (20.46 MHz receiver frequency band). The information is taken from Table 3-Va in IS-GPS-200J (2018)

GPS block	Channel	Signal	
		P(Y)	C/A or L2C
IIA/IIR	L1	− 161.5 dBW	− 158.5 dBW
	L2	− 164.5 dBW	–
IIR-M/IIF	L1	− 161.5 dBW	− 158.5 dBW
	L2	− 161.5 dBW	− 160.0 dBW
III	L1	− 161.5 dBW	− 158.5 dBW
	L2	− 161.5 dBW	− 158.5 dBW

Data and method

GNSS data distributed in RINEX format contain S parameters (Pestana 2015) that represent the carrier-to-noise power density ratio (C/N0) or raw signal strength according to the RINEX 3.03 specification (ftp://igs.org/pub/data/format/rinex303.pdf). The archive of the International GNSS service (IGS, Dow et al. 2019) at (ftp://igs.org/pub/station/general/igs08.atx) presents the schedule of the GPS satellite replacements. For the GPS satellite 10 (PRN10), the replacement of the IIA block with the IIF took place between August 3 and October 31, 2015.

In this work, we used data from the IGS station ZIM2 located in Switzerland (7.47° E; 46.88° N; Fig. 1). Figure 2 shows the C/N0 changes for the GPS signal received at station ZIM2, at L1 (S1) and L2 (S2) on April 29, 2015 (blue dots) and December 27, 2015 (gray and black dots). These dates were specifically chosen outside the interval of the satellite replacement. It should be noted that on these days, there was no hardware update at the receiver. According to the official IGS information, during that time station ZIM2 was equipped with the Trimble NETR9 receiver and the TRM59800.00 antenna (http://www.igs.org/).

The observables for station ZIM2 are taken from files in Rinex3 format. The files contain signal strength observables for the C/A code tracking and the semi-codeless P(Y) z-tracking. We compare S2 observables at the same code (S2W) under z-tracking for both GPS IIA and GPS IIF. Also, we estimate how the signal strength changes when we use the civilian L2C (M+L) tracking.

Figure 2 shows a change at L1 of about 1.5–2.5 dB-Hz when receiving the signal from the modernized IIF satellite and a higher increase of about 3–4.5 dB-Hz for S2W using z-tracking at L2. The signal strength increases by 8.5–20 dB-Hz for the IIF-S2X (as compared to the IIA-S2W) using the L2C (M+L) tracking.

The best way to analyze the effect of the boost in the signal strength would be to compare the received signal power from one satellite during several radio bursts of similar intensity. However, this approach is difficult to implement because powerful radio bursts occur rarely. By analyzing the data over the recent 20 years, Huang et al. (2018) found that, within this period, there occurred only 2384 flares in the L-range, of which only 17 may be classified as severe (10,000 < radio emission flux ≤ 100,000 sfu) and 4 as extreme (radio emission flux > 100,000 sfu). Therefore, in this work, we implement the following approach: we analyze the received signal strength during a flare at a chosen station, which records the C/N0 for satellites of different generations.

The selected events are the September 24, 2011 (Sreeja et al. 2013) and the September 6, 2017 (Yasyukevich et al.
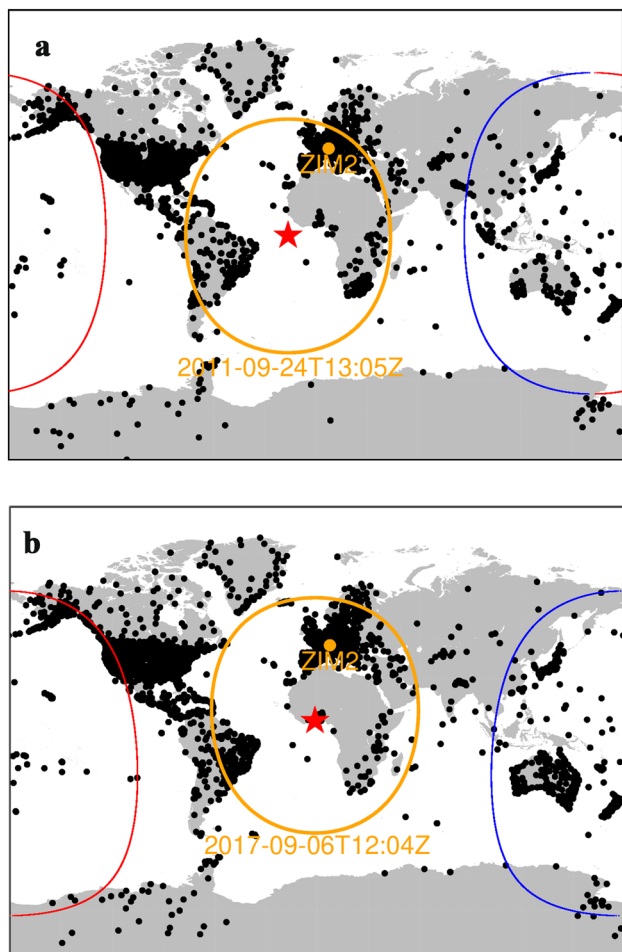
Fig. 1 Geometry of the experiment for the September 24, 2011 (top) and the September 06, 2017 (bottom) SRBs. The big orange dot shows the location of the IGS station ZIM2, the black dots show the worldwide GNSS networks, the red stars show the subsolar points during the maximum intensity of the solar flares, and the orange line confines the area with the solar zenith angle less than 60° (solar elevation >30°). Red and blue lines depict the position of the solar terminator at sunrise (red) and sunset (blue) at the moment of the SRBs maximum emission.

2018a; Berdermann et al. 2018) radio bursts that, according to Huang et al. (2018), are regarded as extreme and severe bursts, respectively. For each flare, we studied the dynamics for the received signal strength at the main (L1) and auxiliary (L2/L5) GPS frequencies at station ZIM2. The analysis was performed for different-generation satellite blocks. We used the S1C and S2W observables, which can be obtained from both "old" GPS block IIA/IIR-A and "new" GPS block IIR-M/IIF. Also, we used S2X observables to estimate code tracking performance at L2, and some data on S5X at L5. A Trimble NETR5 receiver was first installed at ZIM2; however, from April 27, 2015, the Trimble NETR9 version was in operation.

## Solar radio burst of September 24, 2011

To analyze the SRB variations, we used data from the Sagamore Hill spectrograph that is a part of the Radio Solar Telescope Network (RTSN) (ftp://ftp.ngdc.noaa.gov/STP/space-weather/solar-data/solar-features/solar-radio/rstn-1-second/sagamore-hill/). The September 24, 2011 radio emission at 1415 MHz started rising at about 12:32 UT and peaked (114 144 sfu) at 13:05 UT (Fig. 3, red line). Figure 3 shows that the signal strength decreased during the radio burst at the receiver at both L1 (S1) and at L2 (S2) frequencies. According to the RINEX 3.03 specification (ftp://igs.org/pub/data/format/rinex303.pdf) a threshold for good signal tracking is defined as 30-35 dB-Hz. For L1, the C/N0 value threshold for the phase lock to occur is about 28 dB-Hz (Hofmann-Wellenhof et al. 2008). However, special signal post-processing procedures could lower this value to 20 dB-Hz (Psiaki 2001). Therefore, in this work, we take 20 dB-Hz as the threshold level.

At L1, the received signal strengths S1C for both satellites have similar levels, whereas, at L2, the IIA S2W is lower than that at the IIR-M. During the flare peak, the IIA L2 received signal strength S2W drops below 20 dB-Hz, whereas, for the IIR-M, the minimum values of the received signal strength S2W is by 5 dB-Hz higher.

Because the elevation angles for the satellites differ, it is better to compare the received signal strength to the elevation angle (as it was made in Fig. 2). Such comparison is presented in Figure 4 for L1 (S1, left) and for L2 (S2, right). One can see that, for L1, the dependence of the received signal strength S1C on the elevation angle is almost similar for the two blocks. During the flare, we observe a sudden drop of ~7.5 dB-Hz in the signal strength S1C. Such a drop occurs at different satellites for similar elevation angles. However, in general, the received signal strength remains sufficiently high. For L2, however, we observe a difference between the received signal strength for the two blocks: for IIA, the strength level is lower at all elevation angles. During the flare, we observe a decrease in the received signal strength S2W by more than about 17 dB-Hz for both blocks. Due to the initially lower signal power, the IIA minimal value appears below the 20 dB-Hz threshold, which potentially leads to a greater probability of the signal loss of lock during flares. Meanwhile, the decrease in the S2X for the PRN29 (the new block IIR-M) is only of 10 dB-Hz.

Thus, during the flare, we observe a sharp drop in the signal strength of about 7.5 dB-Hz at L1 frequency and of ~17 dB-Hz at L2 frequency when using P(Y) code. However, due to the initially higher L2 signal power on satellites of new type, the signal strength during the flare exceeds the strength of the signal from the "old" satellite. This potentially results in more stable navigation. The flare-induced drop in the signal strength at L2 frequency when using the new civil code
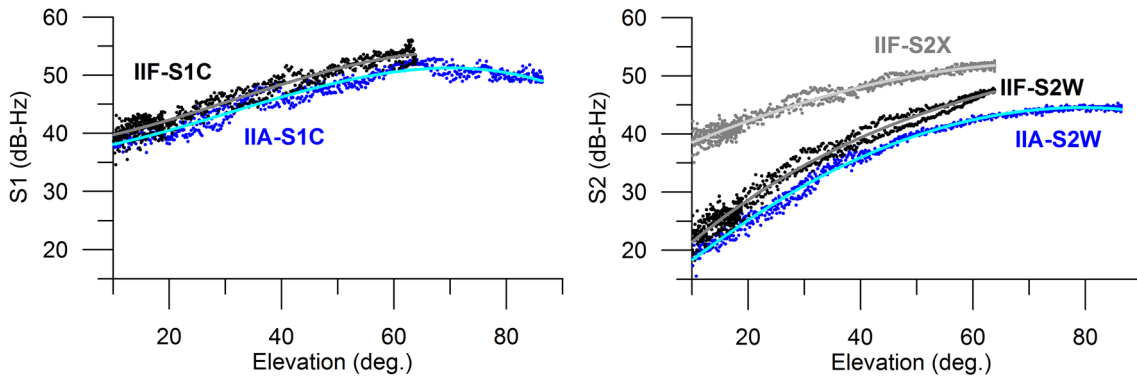
Fig. 2 Elevation angle dependence of GPS PRN10 received signal strength at L1 (left) and L2 (right) for April 29, 2015 (blue dots, GPS IIA) and for December 27, 2015 (gray and black dots, GPS IIF) at ZIM2 station. Black points are for the S1C (left) and S2W (right) from GPS IIF, blue points are for the S1C (left) and S2W (right) from GPS IIA, gray points are for the S2X from GPS IIF. Lines show the corresponding third order polynomial fits.
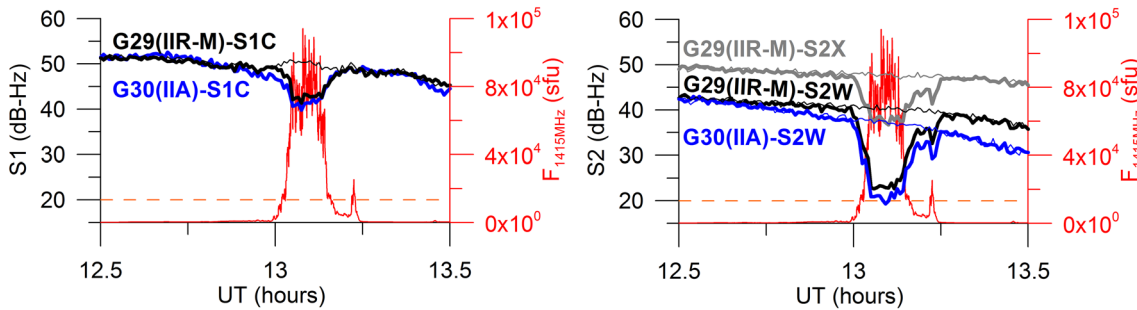
Fig. 3 Solar radio emission at 1415 MHz as recorded by the Sagamore Hill radio spectrograph (red curve) during the September 24, 2011 radio burst, and the signal strength (thick lines) at L1 (left panel) and L2 (right panel) at station ZIM2 for satellites G29 (IIR-M) and G30 (IIA). Black curves correspond to S1C and S2W, blue curves—to S1C and S2W, and gray curves show S2X. Orange dashed line shows a 20 dB-Hz threshold. Thin lines show the signal strengths for reference day (September 23). The reference day data are shifted by 4 minutes to obtain the same geometry of GPS sounding. Note that the same 4-minute time shift is applied for all reference day data throughout the article.
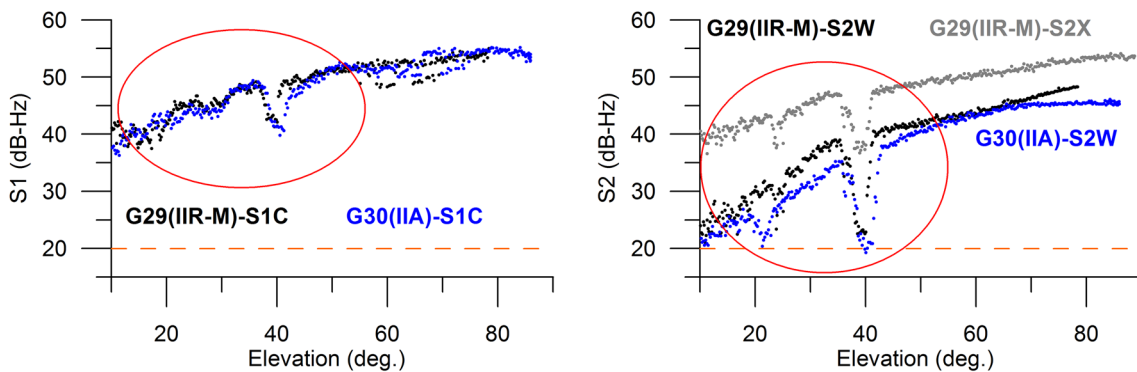
Fig. 4. GPS received signal strength at station ZIM2 at L1 (left panel) and L2 (right panel) during the September 24, 2011 radio burst for two satellites: PRN29 (IIR-M, black and gray dots), PRN30 (IIA, blue dots). Black dots correspond to the S1C (left panel) and to S2W (right panel), blue dots are for S1C (left panel) and S2W (right panel), gray dots are for S2X. Orange dashed line shows the 20 dB-Hz threshold.

is smaller and is comparable with the drop at L1 frequency (about 10 dB-Hz).
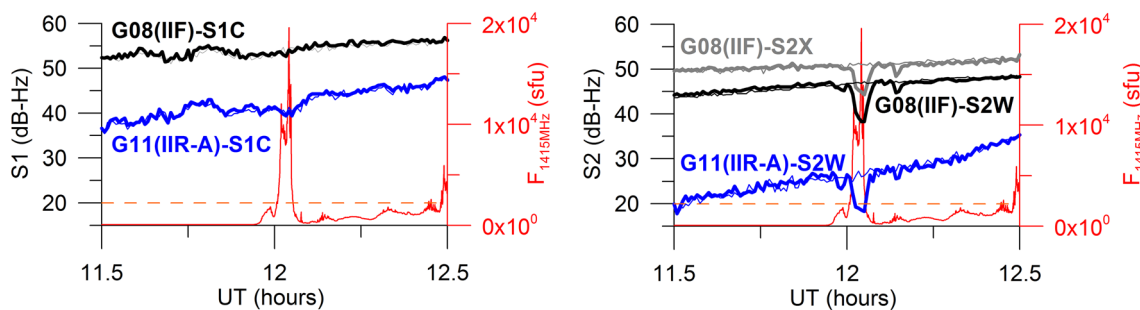
Solar radio burst of September 6, 2017

The September 6, 2017 radio burst accompanied the most powerful X9.3 flare in cycle 24. The maximum value of the radio emission flux reached 19604 sfu at 12:04 UT as obtained from the San Vito radio spectrograph that is a part of the RSTN (ftp://ftp.ngdc.noaa.gov/STP/space-weather/solar-data/solar-features/solar-radio/rstn-1-second/san-vito/).

Figure 5 shows the dynamics of the radio emission flux (red curve). The gray curve shows variations in the received signal strength at ZIM2 from the GPS satellite PRN08 (IIF); the blue one does the same for the GPS PRN11 (IIR-A). One can see that this flare did not affect the measured signal strength S1C at L1. At the same time, the flare caused 8 dB-Hz decrease in the signal strength S2W at L2. This result corresponds to those obtained by Sato et al. (2019) who revealed a decrease in L2, and L5 signal strength up to 10 dB-Hz in the European region. A decrease in L2 signal

strength using civilian L2C code (S2X) is slightly smaller—about 7 dB-Hz.

Figure 6 shows the dependence of the received signal strength on the elevation angle. Unfortunately, during the flare, there were no satellites of different types at similar elevations. However, one can see significant differences in the signal-to-noise ratio at L2. The solar flare effect is in a sharp decrease in the received signal strength at L2. The PRN11 (IIR-A) initially shows lower values for the L2W signal strength (Fig.6, right panel). During the flare, the signal strength dropped down to the 20 dB-Hz threshold level. Note that for the PRN08 (IIF), the radio burst effect was recorded at a higher elevation angle; therefore, a direct comparison of the signal strength from those satellites during the flare is incorrect. Note, however, that the flare-driven total signal strength S2W decrease for both satellites is comparable by amplitude, i.e., ~8 dB-Hz, and does not change with elevation. Therefore, if the radio burst occurred for the PRN08 at the same low elevation angle as for the PRN11, the minimal threshold for PRN08 signal strength would not be reached due to the initially higher power of the L2 P(Y) signal at PRN08. Signal strength for S2X at PRN 08 is higher,

Fig. 5 Dynamics of the solar radio emission at 1415 MHz as recorded by the San Vito spectrograph (red curve) during the September 6, 2017 radio burst and the GPS received signal strength (thick lines) at station ZIM2 for two satellites: G08 (IIF) and G11

(IIR-A). The black curves are for S1C and S2W, blue curves are for S1C and S2W, and the gray curve is for S2X. Thin lines are the signal strengths for the reference day (September 5). Orange dashed line shows the 20 dB-Hz threshold.
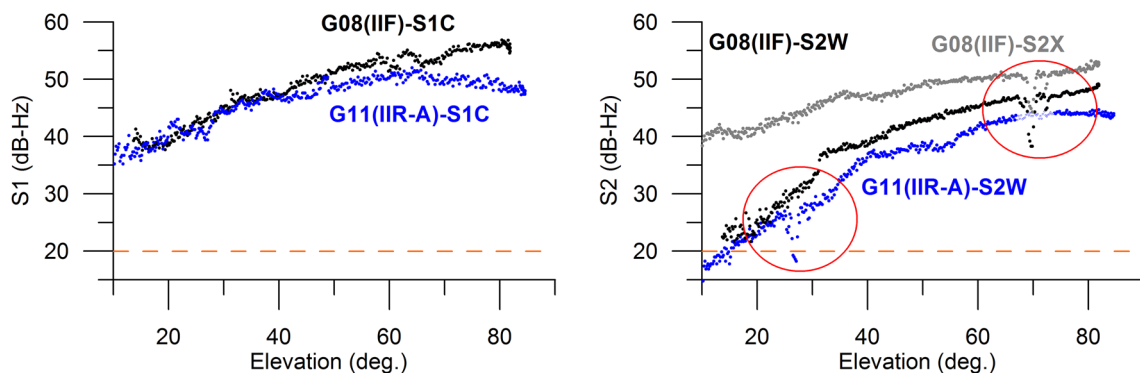
Fig. 6. GPS received signal strength at ZIM2 at L1 (left) and L2 (right) during the September 6, 2017 radio burst for two satellites: PRN08 (IIR-M, black and gray dots), PRN30 (IIR-A, blue dots).

Black dots are for S1C (left) and S2W (right), blue dots are for S1C (left panel) and S2W (right), gray dots are for S2X. Orange dashed lines show the 20 dB-Hz threshold.

especially at low elevation angles and the flare-related effect for this signal is weaker.

Thus, increasing the power of the L2 signal emitted from a satellite can improve the stability of the system against the solar flare threat. However, the use of the new open civil code contributes even greater to the enhancement in the system stability.

The GPS IIF is equipped with a transmitter emitting at L5 frequency. This enables us to analyze the flare effect on different frequencies for the modernized blocks. Figure 7 shows the dynamics for the GPS received signal strength at L1 (S1, black), L2 (S2, gray), L5 (S5, navy blue). The data are for station ZIM2 except for the L5 data in 2011, when ZIM2 did not record L5 observables. Thus, we find another station WTZR (49.14°N; 12.87°E) and put this data on the left panel (see S5-WTZR). In 2011, a Leica GRX1200+GNSS receiver with the LEIAR25. R3 LEIT antenna was installed at station WTZR. However, the WTZR data are only provided in RINEX2 format; therefore we do not have detailed information on observables S5Q, S5I or S5X. In 2011, only two satellites were equipped with the IIF blocks: PRN01 and PRN25. PRN01 was not visible in the region during the flare, while signals from PRN25 were captured at a low elevation of about 15°. Therefore, we used observations S1C, S2W, S2X from PRN29 (IIR-M), and adjusted S5 from PRN25 (IIF). To adjust S5 measurements, we increased all S observables from PRN25 by 5 dB-Hz to match S1C level from PRN29 and PRN25.

Figure 7 shows the strength level of L5 and L1 signals. While we do not observe any decrease in the signal strength in the September 6, 2017 S1C data, the L5 signal strength drop of ~7.5 dB-Hz is comparable, although less pronounced, with the L2 power loss. Our finding is in agreement with the results of Sato et al. (2019), who reported the impact of the September 6, 2017 SRB at GPS L2 and L5 frequencies, but not at L1 frequency. Nevertheless, the use of code tracking (L5 and L2C) decreases the signal strength

as compared to semi-codeless tracking (P(Y)). For instance, during the September 24, 2011 SRB, the L5 signal strength S5 dropped by 9 dB-Hz. Among the considered examples, the P(Y) signal (S2W observable) shows the lowest total power and, therefore, the worst stability during radio bursts.

LoL dynamics during the flares

A decrease in the received signal strength during solar radio bursts often leads to a greater probability of signal losses of lock (e.g., Afraimovich et al. 2009). Here, we analyze how the boost of the emitted signal power at satellites of the new generation affected the general stability of the system operation during solar radio bursts. For this purpose, we estimate the mean density of the GPS signal phase LoL for L1 and L2 during the considered flares. Our results are based on the global GNSS network data that included about 5000 (4659 in 2011 and 4939 in 2017) receivers. The global network includes different global and regional networks such as IGS (Dow et al. 2009), UNAVCO, SONEL, CHAIN (Jayachandran et al. 2009), EUREF (Bruyninx et al. 2012), and SibNet (Yasyukevich et al. 2018b). Fig. 1 shows the distribution of GPS stations that we used in this study. In 2011, data for almost all receivers were provided only in Rinex2 format without information on code tracking type. In 2017, most receivers kept data only in Rinex2 format. Most likely, Rinex2 files contained S1C as S1 and S2W as S2, because if it contained S2X/S2L/S2M as S2, then there was a lot of missing data for "old" GPS satellites that do not emit modernized signals. Wanniger (2018) found that 2.7% of GPS receivers mix L2P(Y)/L2C observations in the Rinex files. We assume that 2.7% is not high enough and should not significantly change the global LoL pattern. Thus, we believe that in our study, the observed differences in the LoL density dynamics for "old" and "new" satellites are associated with the improved emitted signal power rather than with the use of different codes.
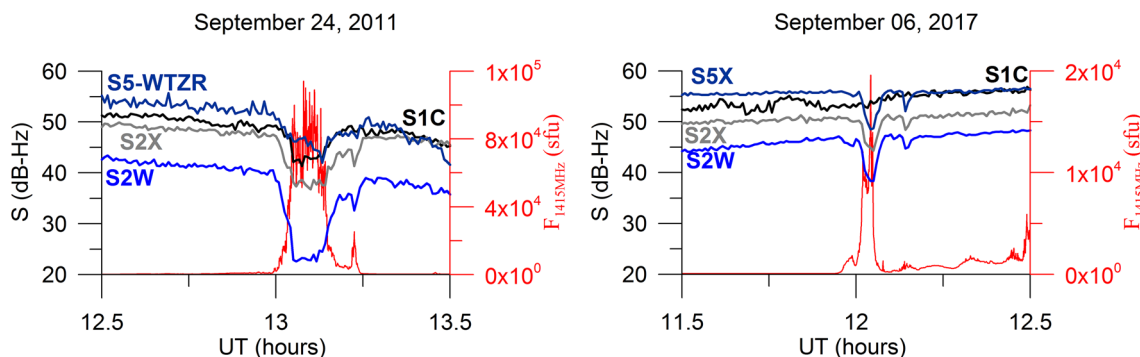
Fig. 7 Dynamics of the strength of GPS received signal S1C (black lines), S2W (blue lines), S2X (gray lines), S5X (navy blue) at station ZIM2. The solar radio emission data for the September 24, 2011

(left panel) and for the September 6, 2017 (right panel) solar flares are shown in red. On the left panel, we show S5 observable at station WTZR (S5-WTZR, navy blue).

We calculated the LoL relative density P_T. For this purpose, at a station, the number of LoL $N(t)$ within the selected time interval t was normalized for the total number of observations $S(t)$. Then, we averaged over all the GPS satellites recorded within this interval (M). Further, we calculated the LoL relative density (percent):

$$P_T = \frac{1}{M} \sum_{j=1}^{M} \frac{N(t)_j}{S(t)_j} \qquad (1)$$

We used data from stations located close to the subsolar region at the flare instant to estimate the LoL density. For this purpose, we consider in (1) only ionospheric pierce points, i.e. line-of-sight (LOS) intersection with the ionosphere at 300 km height, having a solar zenith angle below 60°. This area is marked by orange lines in Fig.1. Finally, we selected only LOS with elevation angles higher than 10°. As a result, we calculated the LoL density separately for the modernized and "old" satellites. At each time instant, the statistics included more than 3000 records for both flares and for both types of satellites.

Figure 8 shows the estimated LoL densities. At all satellites, the LoL density at L2 significantly exceeded that at L1

during the flares. In both cases, the sharp peaks in the LoL densities corresponded to the radio bursts (vertical dashed lines). We do not see such peaks on previous quiet days.

During the 2011 extreme radio burst, a sharp increase in the LoL density at L2 reached 30% of the total number of measurements at the "old" satellites (Fig. 8 bottom left). For the newer satellites, the LoL density maximum value at L2 reached 10% (Fig. 8 top left), which is 20% lower than for the "old" satellites. At L1, the maximum LoL density during the flare grew up to 0.6 % for the modernized satellites and exceeded 1% for the "old" ones. Overall, one may state an essential degradation of the system operation quality during this event. However, the increased power at the new satellites reduced susceptibility to SRB even under semi-codeless treatment.

Figure 8 shows a flare related LoL density increase in 2017, but to a much lesser extent as compared to those in 2011. The maximal values of the LoL density at L2 during the flare reached about 1.6% at the "old" satellites (bottom right), and about 0.8% for the modernized satellites (top right). There was no distinguished effect on L1 LoL density dynamics for this flare. Lesser LoL density during the 2017 SRB is caused, first of all, by a lower intensity of the radio
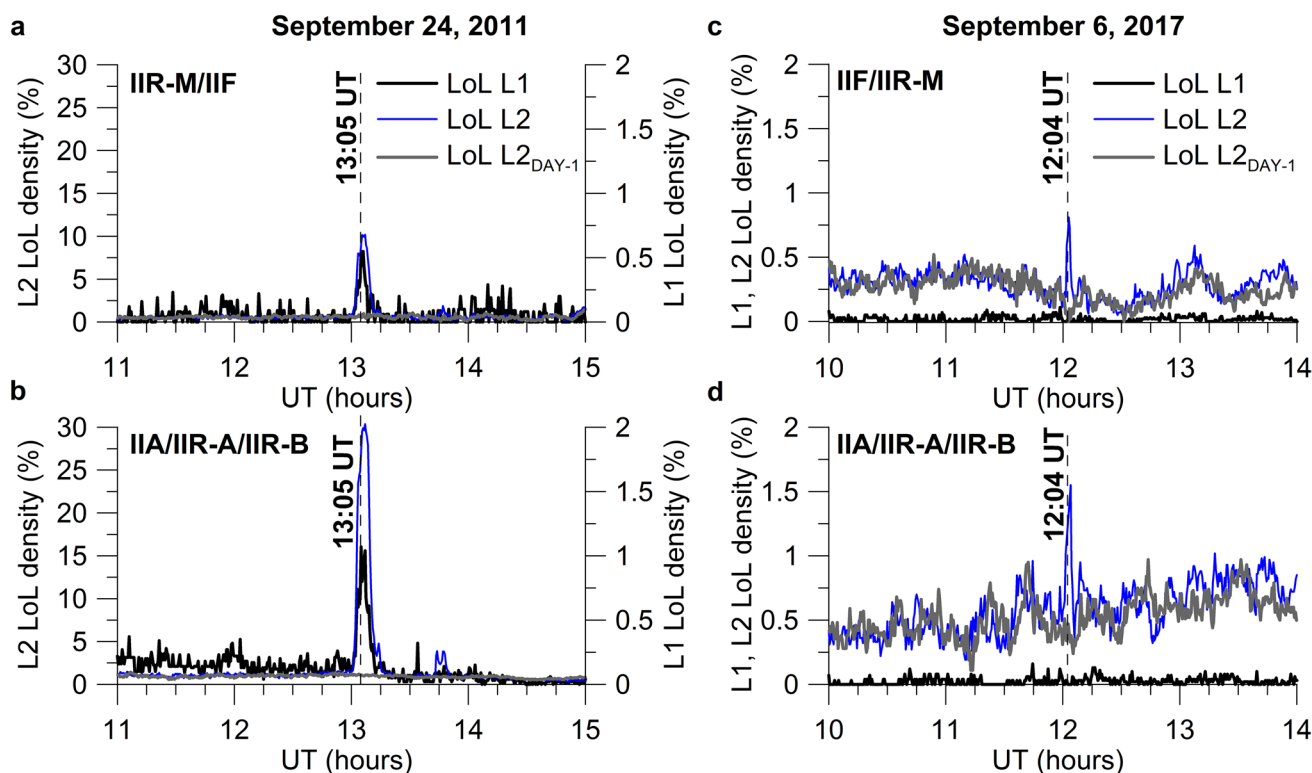
Fig. 8 Density of losses of lock at L1 (black curve) and L2 (blue curve) in the subsolar region during the September 24, 2011 (left) and the September 6, 2017 (right) solar radio bursts for the modernized (top) and "old" (bottom) satellites. Right scales on the left panels are for L1 LoL density in 2011. Bold gray lines show the dynamics of L2 LoL density on previous days. Vertical dashed lines depict the SRBs maxima. Note that for the September 24, 2011 SRB (left panels), we selected the Y-scales for L1 and L2 so that the LoL density levels on the previous day coincided (gray line, top left).

burst. Another factor is the different duration of the disturbance impulse during the flares. Thus, in 2017 the radio flux exceeded a relative threshold value of 5000 sfu for about 2 minutes. In 2011 the threshold was surpassed for more than 10 minutes with a short second peak of about 1 minute. It indicates significant differences between the total disturbing energy amount injected during the flares.

Losses of lock during the September 6, 2017 flare over the European region were studied in detail by Berdermann et al. (2018). Their results indicated that "the space weather event does not coincide with the loss of lock intervals". A smaller number of stations (as compared to the current research) and possibly their better performance could result in the inconsistency with our results shown in Fig. 8. It is interesting to note that Yasyukevich et al. (2018a) found no LoL during the September 2017 flare either. Possible reason for this difference in our results with previous ones could be a different set of stations. The main advance of the current approach is introducing a limit on the solar zenith angle. As we can see from Fig. 1 there are a lot of GPS stations in Europe and America, which are on the sunlit part of the earth. However, most of these stations correspond to low solar elevation (< 60°). At stations with low solar elevation, SRB did not impact the losses of lock. Therefore, in previous studies, adding stations with low elevation could "hide" the effect. Our new approach allowed us to reveal the effect.

Both the satellite elevation and the solar zenith angle should influence the loss of lock density: lower signal strength at low elevation increases the LoL probability, and so does higher emission flux at low zenith angles. The top panel in Fig. 9 demonstrates the LoL density at L2 depending on the elevation and solar zenith angles during the 10-min period around the peak of the 2011 SRB. The figure confirms that during the flare most of LoLs occur at low zenith angles, generally less than 40°. It is interesting to note that for this powerful flare we observe losses of lock at zenith angles around 30°, i.e., even at high satellite elevations.

Middle and bottom panels in Fig. 9 show the LoL densities at L1 (black curves) and L2 (blue curves) for the modernized (solid lines) and "old" (dashed lines) satellites. LoLs are calculated for the 10 min periods around the peaks of the September 24, 2011 (middle) and the September 6, 2017 (bottom) solar radio bursts, respectively. We do not show here LoL dynamics at L1 during the 2017 SRB, because of a small number of the LoLs recorded during this event. This did not allow us to obtain reliable results. During both flares, the LoL density at L2 (for both modernized and "old" satellites) depends on solar zenith angle. However, at L1 in 2011 this dependency is not clear enough. We could use the dependencies to predict losses of phase lock probability under SRB. The supplementary materials contain the temporal evolution of the LoLs
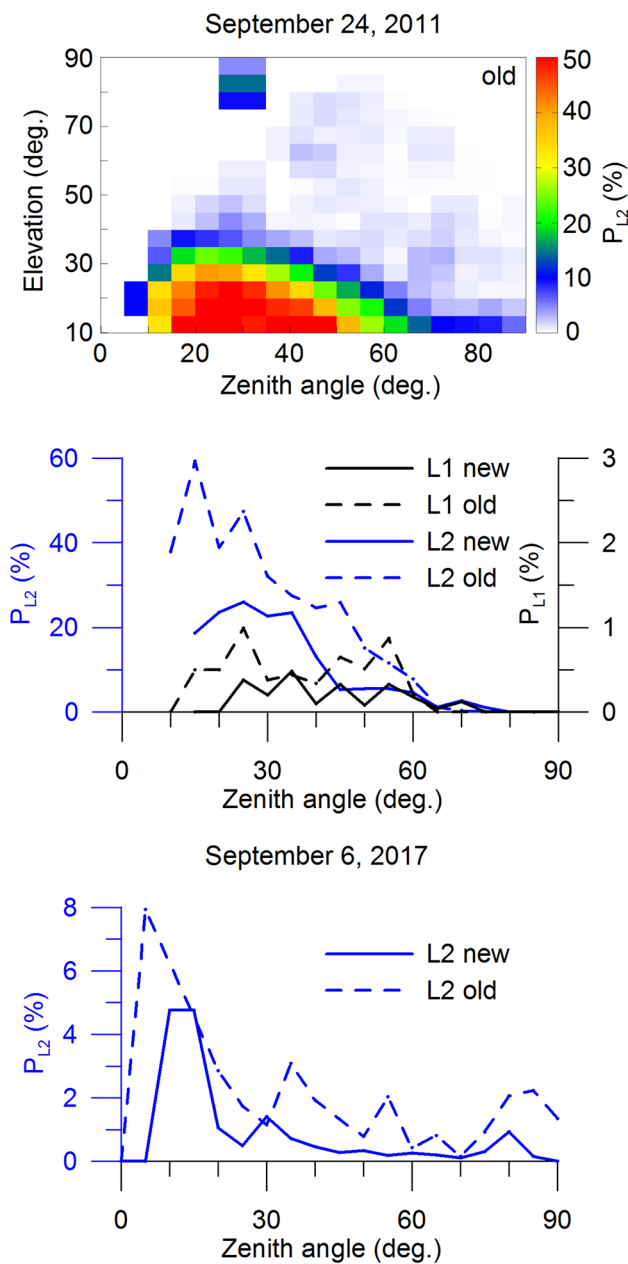
Fig. 9 Loss of lock density vs. the satellite elevation and the solar zenith angle. Top panel shows 2D-distribution of LoL density at L2 vs. the elevation and the solar zenith angle for the 2011 solar radio burst. Middle and bottom panels shows LoL density dynamics vs. the solar zenith angle for the 2011 SRB and the 2017 SRB, correspondingly: black marks L1 data, blue marks L2 data, solid lines corresponds to the modernized satellites and dashed lines correspond to "old" satellites. All calculations are made for the 10 min periods around the SRB peaks.

depending on the solar zenith angle at both modernized and "old" satellites during the flares. All this also confirms strong LoL dependence on the solar zenith angle and the better tracking stability of signals from the modernized satellites during a flare.

In both cases, the L2 LoL density decreased more than twice at the modernized satellites. Hence, one may conclude that the increased emitted signal power at the modernized satellites improves the system stability with respect to both severe and extreme solar radio bursts.

Summary and conclusion

In this work, we analyzed how the increase in the emitted signal power at modernized GPS satellites affected the system operation stability during the extreme (September 24, 2011) and severe (September 6, 2017) solar radio bursts. We showed that, after the IIA/IIR-A blocks were replaced with IIR-M/IIF modernized ones, the signal strength S2W at L2 frequency increased by about 3–4.5 dB-Hz at station ZIM2. Even a stronger increase in signal power was observed for the modernized L2C code (S2W observables): the increase reached 20 dB-Hz compared with the IIA S2W. During the considered solar radio bursts, the navigation signal strength decreased at L2 and L5 for semi-codeless z-tracking (S2W) and code tracking (S2X, S5X). Herewith, the L2 signal under semi-codeless P(Y) z-tracking features the least total power (S2W) and, thereupon, the worst stability during the radio bursts. Also, it is S2W that corresponds to the maximum drop of signal strength during an SRB. During the 2011/2017 SRBs the signal strength drops were: 7.5/0 dB-Hz for S1C, 10/7 dB-Hz for S2X, 9/7.5 for S5/S5X, 17/8 dB-Hz for S2W for the corresponding SRBs peaks. Thus, more intensive SRB corresponds to a higher drop in signal strength. We should note that using civilian codes enables us to decrease the signal strength drop under solar radio bursts.

Drop in the signal strength S2W for the modernized blocks was comparable in amplitude to those of "old" blocks. However, IIR-M/IIF recorded about 5 dB-Hz higher signal strength. This difference does not depend on the receiver and antenna type. This potentially results in more stable navigation.

By analyzing the GPS L1/L2 signal loss of locks during both SRBs we showed that the LoL density at L2 at modernized satellites was lower than that at the "old" satellites. During the extreme SRB, the LoL density at "old" satellites reached 30%, which is 3 times higher than at modernized satellites. The corresponding values for the severe SRB were 1.6% and 2 times. Therefore, the enhanced power of the emitted signals improves the signal tracking at GPS. During the September 24, 2017 extreme SRB we also detected an increase in LoL density at L1 frequency for both types of satellites. Meanwhile, there was no obvious effect on L1 LoL density during the September 6, 2017 severe SRB.

We must emphasize that we did not compare the effects of the 2011 and 2017 flares in our study. For each case, we separately analyze the stability of signals from "old" and "new" satellites received at the same station (respectively, on the same equipment and software). Also, we do not aim to determine which mechanism—SITEC or SRB—is prevalent in producing the LoLs during the flares. Therefore, without entering into an argument about the main impact, our results prove that the increase in the emitted signal power at modernized satellites improves the system stability with respect to the threats from both severe and extreme flares accompanied by solar radio bursts. Modernized signals also can improve stability.

References

Afraimovich EL, Demyanov VV, Kondakova TN (2003) Degradation of GPS performance in geomagnetically disturbed conditions. GPS Solut 7(2):109–119. https://doi.org/10.1007/s10291-003-0053-7

Afraimovich EL et al (2013) A review of GPS/GLONASS studies of the ionospheric response to natural and anthropogenic processes and phenomena. J Space Weather Space Clim 3:A27. https://doi.org/10.1051/swsc/2013049

Afraimovich EL, Demyanov VV, Smolkov GY (2009) The total failures of GPS functioning caused by the powerful solar radio burst on December 13, 2006. Earth Planets Space 61:637–641. https://doi.org/10.1186/BF03352940

Ashjaee J, Lorenz R (1992) Precision GPS surveying after Y-code. In: Proc. ION GPS 1992, Institute of Navigation, Albuquerque, NM, USA, September 16-18, 657-659

Astafyeva E, Yasyukevich Y, Maksikov A, Zhivetiev I (2014) Geomagnetic storms, super-storms, and their impacts on GPS-based navigation systems. Space Weather 12(7):508–525. https://doi.org/10.1002/2014SW001072

Berdermann J, Kriegel M, Banys D, Heymann F, Hoque MN, Wilken V, Borries C, Heßelbarth A, Jakowski N (2018) Ionospheric response to the X9.3 Flare on September 6 2017 and its implication for navigation services over Europe. Space Weather 16:1604–1615. https://doi.org/10.1029/2018SW001933

Bruyninx C, Habrich H, Söhne W, Kenyeres A, Stangl G, Völksen C (2012) Enhancement of the EUREF permanent network services and products. Geodesy Planet Earth IAG Symp Ser 136:27–35. https://doi.org/10.1007/978-3-642-20338-1_4

Carrano CS, Bridgwood CT, Groves KM (2009) Impacts of the December 2006 solar radio bursts on the performance of GPS. Radio Science 44(1):RS0A25. https://doi.org/10.1029/2008RS004071

Cerruti AP, Kintner PM, Gary DE, Lanzerotti LJ, de Paula ER, Vo HB (2006) Observed solar radio burst effects on GPS/Wide area augmentation system carrier-to-noise ratio. Space Weather 4(10):S10006. https://doi.org/10.1029/2006SW000254

Chen Z, Gao Y, Liu Z (2005) Evaluation of solar radio bursts' effect on GPS receiver signal tracking within international GPS service network. Radio Science 40:RS3012. https://doi.org/10.1029/2004RS003066

Coster A, Komjathy A (2008) Space weather and the global positioning system. Space Weather 6:S06D04. https://doi.org/10.1029/2008SW000400

Demyanov VV, Yasyukevich YUV, Jin S (2013) Effects of solar radio emission and ionospheric irregularities on GPS/GLONASS performance. In: Jin S (ed) Geodetic sciences—observations modeling and applications. Intech, London, pp 177–122. https://doi.org/10.5772/3439

Dow JM, Neilan RE, Rizos C (2009) The international GNSS service in a changing landscape of global navigation satellite systems. J Geodesy 83:191–198. https://doi.org/10.1007/s0019000803003

Fortes LPS, Lin T, Lachapelle G (2015) Effects of the 2012–2013 solar maximum on GNSS signals in Brazil. GPS Solut 19:309–319. https://doi.org/10.1007/s10291-014-0389-1

Hofmann-Wellenhof B, Lichtenegger H, Wasle E (2008) GNSS–Global navigation satellite systems: GPS, GLONASS, Galileo & more. Springer, Vienna

Huang W, Ercha A, Shen H, Liu S (2018) Statistical study of GNSS L-band solar radio bursts. GPS Solut 22:114. https://doi.org/10.1007/s10291-018-0780-4

IS-GPS-200J (2018) Global positioning systems directorate. Systems engineering & integration interface specification IS-GPS-200, https://gps.gov/technical/icwg/IS-GPS-200J.pdf

Jakowski N, Stankov SM, Klaehn D (2005) Operational space-weather service for GNSS precise positioning. Ann Geophys 23:3071–3079. https://doi.org/10.5194/angeo-23-3071-2005

Jayachandran PT, Langley RB, MacDougall JW et al (2009) The Canadian high arctic ionospheric network (CHAIN). Radio Sci 44:RS0A03. https://doi.org/10.1029/2008RS004046

Jin Y, Oksavik K (2018) GPS scintillations and losses of signal lock at high latitudes during the 2015 St. Patrick's Day storm. J Geophys Res Space Phys 123:7943–7957. https://doi.org/10.1029/2018JA025933

Klobuchar JA, Kunches JM, Van Dierendonck AJ (1999) Eye on the ionosphere: potential solar radio burst effects on GPS signal to noise. GPS Solut 3(2):69–71. https://doi.org/10.1007/PL00012794

Matsoukas D, Papagiannis M, Aarons J, Klobuchar J (1972) Correlation of solar radio bursts and sudden increases of the total electron content (SITEC) of the ionosphere. J Atmos Terr Phys 34(7):1275–1283. https://doi.org/10.1016/0021-9169(72)90137-7

Muhammad B, Alberti V, Marassi A, Cianca E, Messerotti M (2015) Performance assessment of GPS receivers during the September 24, 2011 solar radio burst event. J Space Weather Space Clim 5:A32. https://doi.org/10.1051/swsc/2015034

Pestana A (2015) Technical report: reading RINEX 2.11 observation data files. https://doi.org/10.13140/RG.2.1.4888.4087

Psiaki ML (2001) Block acquisition of weak GPS signals in a software receiver. In: Proc. ION GPS 2001, Salt Lake City, UT, September 11-14, pp 2838-2850

Rodríguez-Bilbao I, Radicella SM, Rodríguez-Caderot G, Herraiz M (2015) Precise point positioning performance in the presence of the 28 October 2003 sudden increase in total electron content. Space Weather 13:698–708. https://doi.org/10.1002/2015SW001201

Sato H, Jakowski N, Berdermann J, Jiricka K, Heßelbarth A, Banyś D, Wilken V (2019) Solar radio burst events on September 6 2017 and its impact on GNSS signal frequencies. Space Weather 17:816–826. https://doi.org/10.1029/2019SW002198

Sreeja V, Aquino M, Jong K (2013) Impact of the September 24 2011 solar radio burst on the performance of GNSS receivers. Space Weather 11:306–312. https://doi.org/10.1002/swe.20057

Sreeja V, Aquino M, Jong K, Visser H (2014) Effect of the September 24 2011 solar radio burst on precise point positioning service. Space Weather 12(3):143–147. https://doi.org/10.1002/2013SW001011

Tsurutani BT, Verkhoglyadova OP, Mannucci AJ, Lakhina GS, Li G, Zank GP (2009) A brief review of '"solar flare effects"' on the ionosphere. Radio Sci 44:RS0A17. https://doi.org/10.1029/2008RS004029

Wan W, Liu L, Yuan H, Ning B, Zhang S (2005) The GPS measured SITEC caused by the very intense solar flare on July 14, 2000. Adv Space Res 36:2465–2469. https://doi.org/10.1016/j.asr.2004.01.027

Wanninger L (2018) Detection of RINEX-2 files with mixed GPS L2P(Y)/L2C carrier phase observations. Sensors 18(12):4507. https://doi.org/10.3390/s18124507

Yasyukevich Y, Astafyeva E, Padokhin A, Ivanova V, Syrovatskii S, Podlesnyi A (2018) The September 6 2017 X-class solar flares and their impacts on the ionosphere, GNSS, and HF radio wave propagation. Space Weather 16:1013–1027. https://doi.org/10.1029/2018SW001932

Yasyukevich YuV, Vesnin AM, Perevalova NP (2018) SibNet–Siberian global navigation satellite system network: current state. Solar-Terr Phys 4(4):63–72

Zakharov VI, Yasyukevich YuV, Titova MA (2016) Effect of magnetic storms and substorms on GPS slips at high latitudes. Cosmic Res 54(1):20–30. https://doi.org/10.1134/S0010952516010147

Zhang DH, Xiao Z (2005) Study of ionospheric response to the 4B flare on October 28 2003 using international GPS service network data. J Geophys Res 110:A03307. https://doi.org/10.1029/2004JA010738

Zhang SR, Coster AJ, Erickson PJ, Goncharenko LP, Rideout W, Vierinen J (2019) Traveling ionospheric disturbances and ionospheric perturbations associated with solar flares in September 2017. J Geophys Res Space Phys 124:5894–5917. https://doi.org/10.1029/2019JA026585

Yu. V. Yasyukevich received his Ph.D. degree in Radio Physics from ISTP SB RAS in 2009. He works at the ISTP SB RAS as a leading researcher and the Irkutsk State University as an Associate Professor. His scientific interests include monitoring and modeling based on GNSS data, space weather impact on GPS/GLONASS, estimating the absolute total electron content, and ionospheric anomalies. He is the PI of the SIMuRG project (http://simurg.iszf.irk.ru).

A. S. Yasyukevich received her Ph.D. degree in Physics of the Atmosphere and Hydrosphere at the Institute of Solar-Terrestrial Physics SB RAS in 2015. She works at the ISTP SB RAS as a scientific researcher. Her scientific interests are space weather impact on GNSS, ionospheric morphology and neutral atmosphere-ionosphere coupling.

E. I. Astafyeva received her Ph.D. at the Institute of Solar-Terrestrial Physics (Siberian Branch, Russian Academy of Sciences) in 2005. She has been a tenured CNRS researcher at the Institute of Physics of the Earth of Paris (IPGP) since 2012. Her main interests include ionospheric response to natural hazards, geomagnetic, ionospheric and thermospheric storms, and space weather.